

RESEARCH

Open Access

# Correction of wavefront rotation between interferometer and shack-hartmann sensor using bending modes



Yi Zhu<sup>1,2\*</sup> , Tao Chen<sup>2</sup> and Hongzhuang Li<sup>2</sup>

## Abstract

In some active optics system, the influence function, which is the surface deformation ability of an actuator, is measured by directly detecting the mirror surface using an interferometer and the surface correction of the primary mirror is done using the Shack-Hartmann (S-H) sensor. However, if the wavefronts of the interferometer and the S-H sensor have an obvious rotation, a large error will be introduced to the correction force calculations. In this paper, bending modes are used to detect this wavefront rotation. Bending modes are a series of orthonormal stiffness-increasing modes calculated using the influence functions. Two methods, optimum search and top-line (a line passes through the surface center and the top of surface deformation peaks) detection, are developed and tested in simulation using the experimental data of a 620-mm active optics system. The detection errors of the two methods are  $0.286^\circ$  and  $0.085^\circ$  in the simulation, respectively. The rotation detection method is then tested on this 620-mm system. The simulation and experimental results show that top-line detection is a suitable method for the detection of wavefront rotation.

**Keywords:** Wavefront rotation; active optics, Bending mode

## Introduction

Measurements of influence functions, which help finding the surface deformation ability of an actuator, consumes large amount of time. For example, in the active optics system of a 4 m SiC mirror in our lab, there are 54 actuators; and it therefore needs at least 540 min for a loop of influence function measurement (about 5 min for each force application and surface detection and at least twice of these for one actuator). Such measurement requires a time-consuming stable detection condition, so the mirror surface is planned to be directly detected by a Zygo interferometer in a closed detection tower during the influence function measurement to obtain a high precision result. After this measurement, the mirror surface is detected by the S-H sensor of the active optics system. Then the problem left is that the wavefronts detected by the interferometer and the S-H sensor may have a rotation angle. If the angle is larger than  $1.0^\circ$ , it

will obviously hamper the correction ability of the active optics system. Hence, wavefront rotations should be detected and adjusted before active corrections. On the other hand, it is also difficult to include additional components in the system just for detecting such rotations. Therefore, detections of wavefront rotations without additional components are necessary for surface corrections.

Bending modes are first used on the active optics system of Starfire Optical Range Telescope (SORT), and then successfully applied on other active optics systems [1–5]. They are a series of orthonormal modes created via singular value decomposition (SVD) on the influence matrix of the actuators. Mode stiffness is arranged in an increasing order, and mode surfaces can be properly rebuilt on the mirror of the active optics system. Therefore, we apply the first order bending mode of the system to detect wavefront rotations and the rotation detections are tested on a 620-mm active optics experimental system in our lab.

The primary mirror of the above-mentioned active optics experimental system is a 620-mm thin meniscus

\* Correspondence: [13998211017@139.com](mailto:13998211017@139.com)

<sup>1</sup>Changchun Institute of Optics, Fine Mechanics and Physics, Chinese Academy of Sciences, Dong Nan Hu Road 3888, Changchun 130033, China

<sup>2</sup>University of Chinese Academy of Sciences, Beijing 100049, China

mirror with a 170-mm hole in the center. It has 36 active axial supports and 6 passive lateral supports and the axial supports are arranged in three rings. The active axial support is provided by mechanical force actuators, as shown in Fig. 1. The system is detected in horizontal state while the gravity is balanced by the lateral supports and only surface corrections are performed by the active axial supports.

The primary mirror surface is detected by an S-H wavefront sensor that is shown in Fig. 2. It contains a camera, a light source, a beamsplitter, a lenslet and two collimation lenses. This sensor sends a spherical lightwave to the primary mirror and collimates the reflected light to the lenslet to acquire a dot image and to calculate the wavefront. The lenslet has a pitch of 300 μm and a focal length of 7 mm, which results in a wide detection range to deal with the large astigmatism of the primary mirror aberration in the passive support state. The system has 272 sample points that are fitted to 32 Zernike polynomials, excluding two tilts and defocus. Zernike polynomials are useful in expressing wavefront data [6, 7].

**Bending mode correction strategy**

**Influence function**

The influence function, which is the surface deformation ability of an actuator, is the basis of the bending mode correction. However, a one point-force can only cause rigid movement. To avoid rigid movement and create a surface deformation, the net force and net moment should be balanced. This means that.

$$\sum_{i=1}^n f_i = 0, \quad \sum_{i=1}^n f_i \cdot x_i = 0, \quad \sum_{i=1}^n f_i \cdot y_i = 0, \quad (1)$$

where  $f_i$  is the active force added on the  $i$ th actuator, and  $f_i \cdot x_i$  and  $f_i \cdot y_i$  are  $x$ -axis and  $y$ -axis moment of the  $i$ th actuator, where  $x_i$  and  $y_i$  are the coordinates of the actuator. This means that at least

three more actuators are needed to balance the net force and net moment.

The balance force is distributed on all actuators and minimized in RMS, and the net force is equally distributed over all the actuators. The net moment is distributed in proportion to the actuator coordinates, referring to the Multiple Mirror Telescope [2]. For a force vector  $F_i$ , which is  $f$  N on the  $i$ th actuator and 0 N on other actuators, the balance force vectors are.

$$\begin{aligned} F_N &= (f/n) * E \\ F_X &= (f \cdot x_i) * \left( X / \sum_{i=1}^n x_i \right) \\ F_Y &= (f \cdot y_i) * \left( Y / \sum_{i=1}^n y_i \right), \end{aligned} \quad (2)$$

where  $X$  and  $Y$  are the vectors of coordinates  $x$  and  $y$ , and  $F_N$ ,  $F_X$  and  $F_Y$  are the balance force vectors for net force and net moment of the  $x$ -axis and  $y$ -axis. If  $X$  and  $Y$  satisfy.

$$\sum_{i=1}^n x_i = 0, \quad \sum_{i=1}^n y_i = 0, \quad \sum_{i=1}^n x_i \cdot y_i = 0, \quad (3)$$

then  $F_N$ ,  $F_X$ , and  $F_Y$  are independent and the balanced force of  $F_i$  is  $F_i - F_N - F_X - F_Y$ . Actuators set at the regular position commonly satisfy Eq. 3, which is the case for the 620-mm active optics system.

The influence force of each actuator is obtained by adding a unit force on this actuator and balancing the force on all actuators by using the former method. The rank of the influence force matrix is three less than the number of actuators because of the balance distribution. Therefore, the rank of the influence matrix is also three less than the number of actuators.

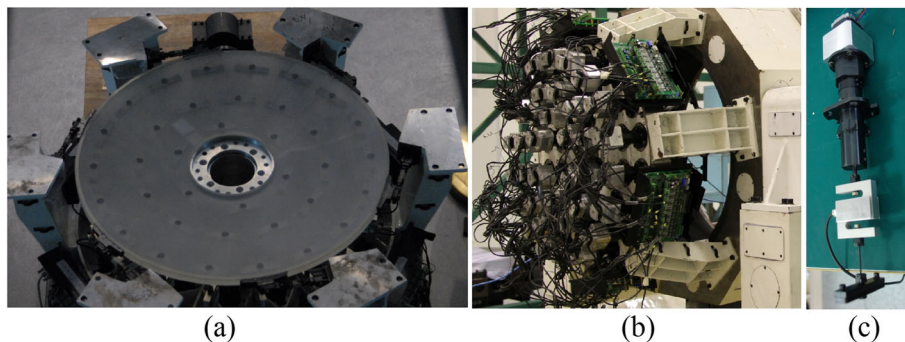


**Fig. 1** 620 mm primary mirror (a), active support system (b), and actuator (c)

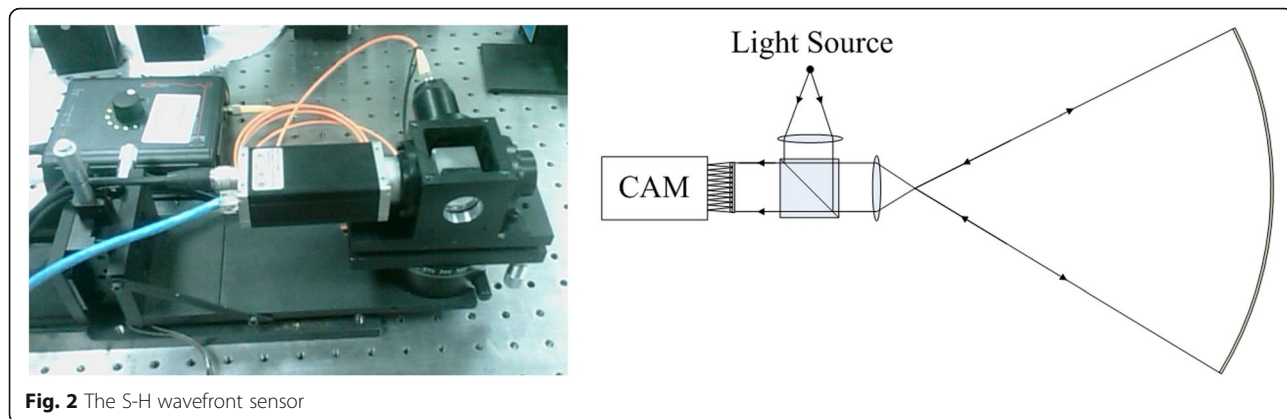


Fig. 2 The S-H wavefront sensor

**Bending mode**

As the basis of the primary mirror surface correction, the active force  $F$  added on the active support causes a surface aberration  $W$ :

$$W = A*a, \quad F = F_A*a, \tag{4}$$

where  $A$  is the influence matrix of the actuators,  $F_A$  is the influence force matrix, and  $a$  is calculated by a least squares fitting such as  $a = (A^T A)^{-1} A^T * W$ . However, the correction may require many iteration steps to acquire an acceptable surface, and the correcting force may be too large to add onto the actuators. To obtain a suitable correcting force, a better fitting base than the influence function is needed.

Bending modes are a series of orthonormal modes converted from the influence matrix  $A$ . The mode matrix  $B$  is obtained by performing SVD on  $A$ , such as.

$$A = B*S*V^T, \quad B = A*V*S^{-1}. \tag{5}$$

$B$  is a combination of the influence matrix  $A$ , so the mode surface can be properly rebuilt on the primary mirror by using its mode force. The mode force  $F_B$  is defined as

$$F_B = F_A*V*S^{-1}. \tag{6}$$

Since  $B$  is orthonormal, the mode coefficients  $b$  and the correcting force  $F$  are.

$$b = B^T*W, \quad F = F_B*b. \tag{7}$$

The columns of  $F_B$ , which are mode force vectors related to bending modes, are arranged in an increasing order [2, 8]. This means that lower order mode deformation occurs more easily, and fitting a surface aberration by low order modes could effectively optimize the correcting force amplitude with an acceptable fitting precision.

Figure 3 shows the first 6 bending modes of the 620 mm active support system. Mode #1 and mode #2 are similar to astigmatism and these two modes are easily to be produced by the active optics system.

Further discuss about the orthonormality of bending mode in Zernike base is shown in Appendix.

**Wavefront rotation detection**

A high precision influence matrix measurement is usually performed using a detection system directly aimed at the primary mirror using a high-quality light source. This high-precision influence matrix is then used in the active optics system. Then, the S-H wavefront sensor of the active optics system detects the primary surface deformation. However, if the wavefront has an obvious rotation with respect to the influence matrix, the correction ability will be largely deteriorated.

Since the active optics system detects primary mirror deformations, the detection of a specific deformation could aid in determining the wavefront rotation. This detection requires no additional measurement components. A unique mirror deformation such as the influence of one actuator could perform this function, but the low-order bending mode is much more ‘soft’ that a small mode force can make a large deformation for detection. Moreover, the low-order mode surface has a low spatial frequency that is easily detected and introduces less detection error. Therefore, using the first order mode could result in high-precision detection.

As mentioned in Section 2.2, the mode surface could be precisely rebuilt on the primary mirror by adding its mode force on the actuators. Then, the detection is performed by adding a mode force on the support, detecting the wavefront of the rebuilt mode, and comparing

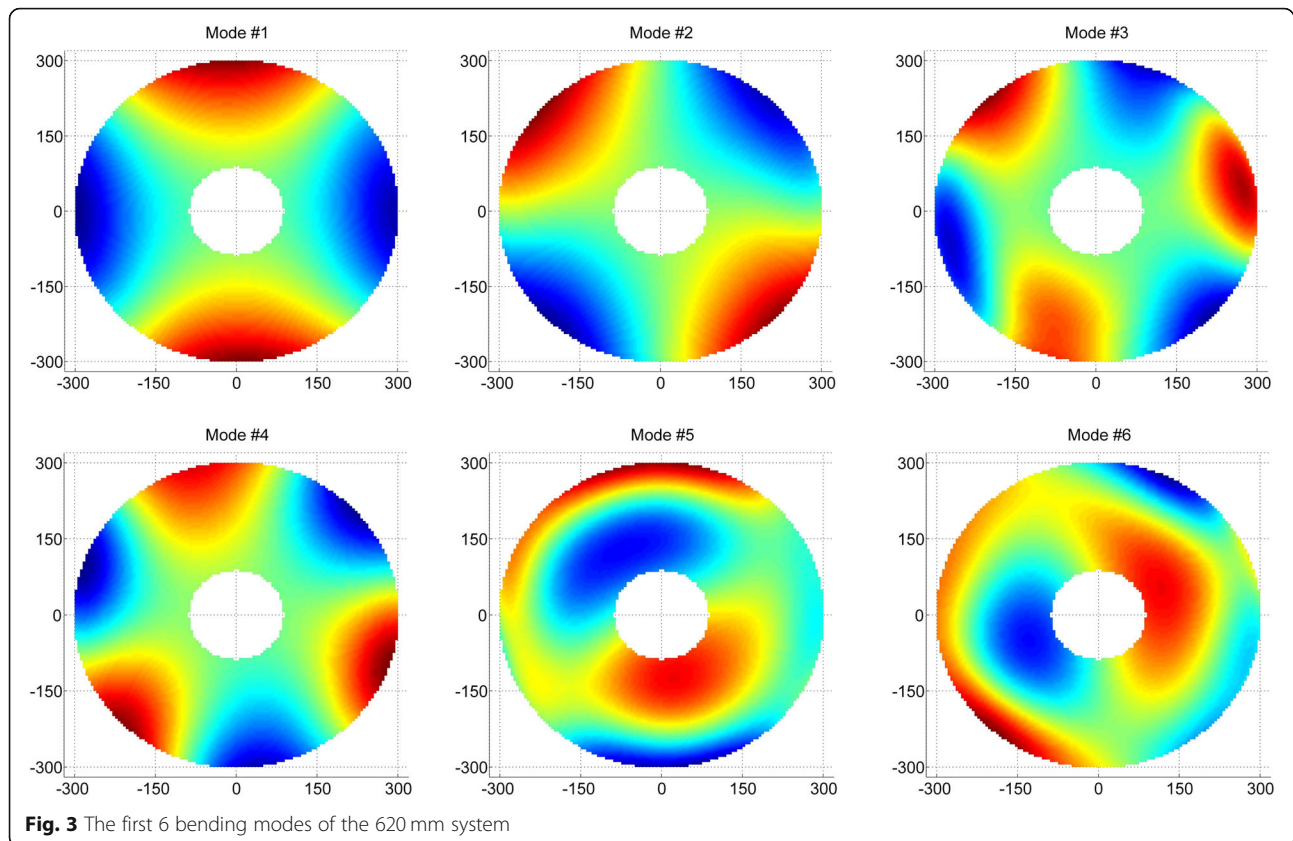


**Fig. 3** The first 6 bending modes of the 620 mm system

the wavefront surface with the mode surface to determine the rotation angle.

For a regular structure support system, the first order bending mode is like an astigmatism, which has two symmetric valleys and peaks. Therefore, the rotation  $\alpha$  detected using this mode can be either of two symmetric rotations:  $\alpha$  and  $180^\circ + \alpha$ . An additional detection is needed to ensure that the true result is obtained, using an asymmetric surface, such as the influence function of one actuator or an asymmetric low order mode.

#### Zernike coefficient rotation

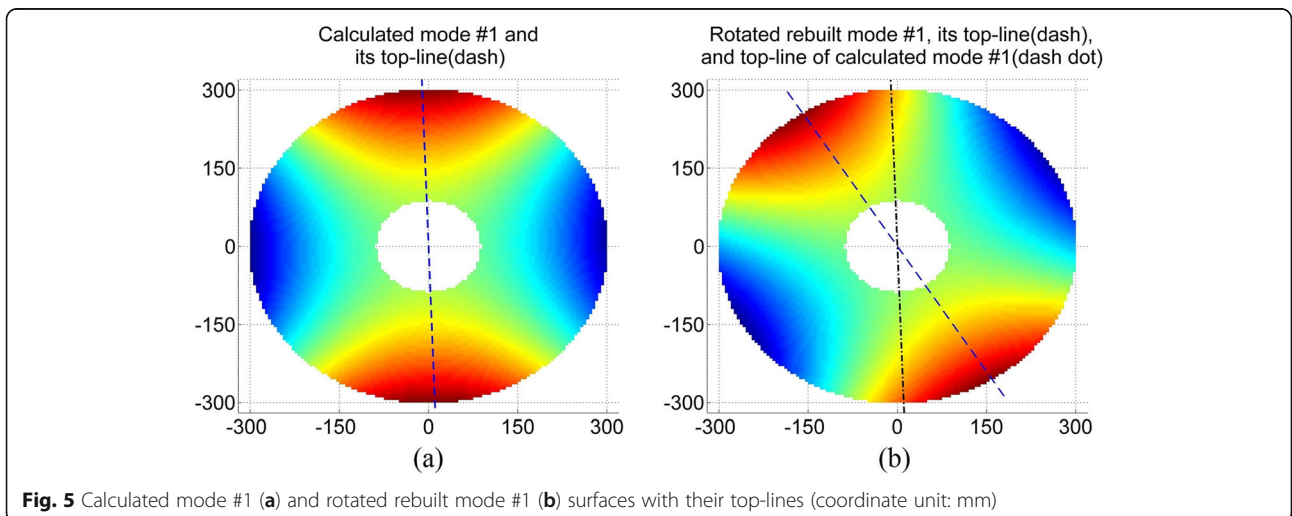
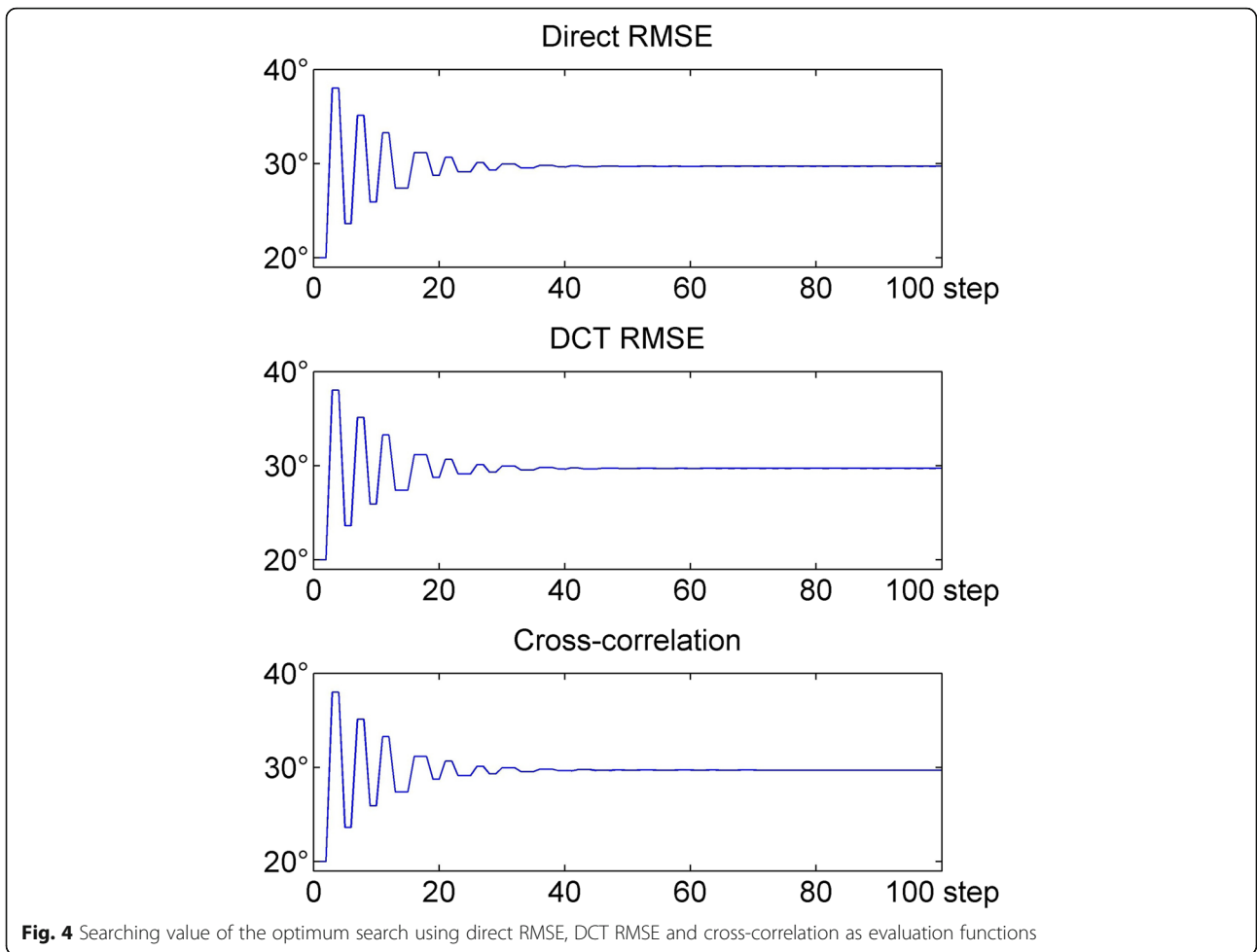
The detected wavefront of the S-H wavefront sensor is described in terms of Zernike coefficients. The Zernike coefficients are easy to be rotated since all the Zernike polynomials are circularly symmetric or orthogonal in pairs. Rotation of orthogonal polynomial pairs is performed by multiplying a rotation matrix with their coefficients. The angle of the rotation matrix is equal to the phase angle of the Zernike polynomial pair, which is equal to the rotation angle multiplied by the rotation order of the

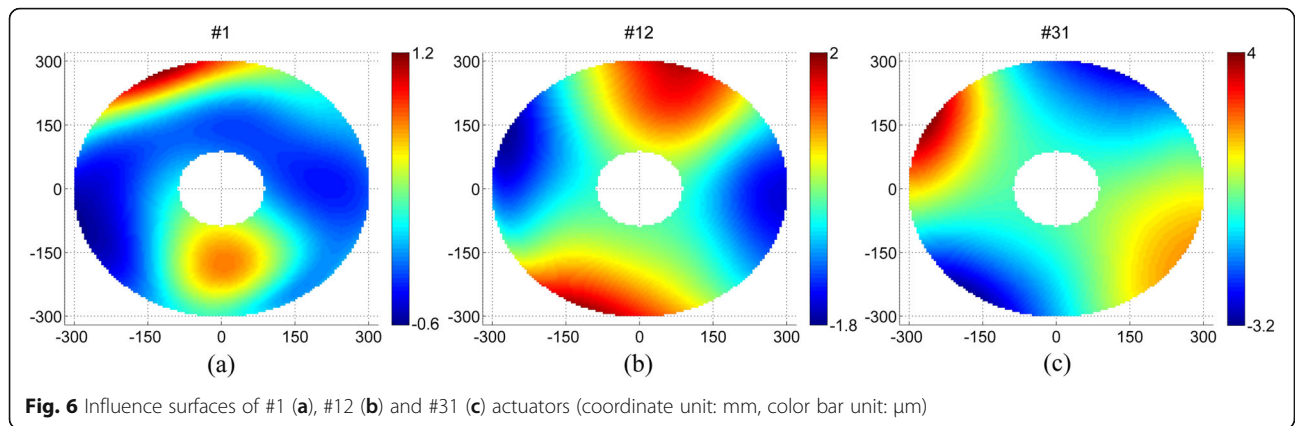
Zernike polynomial. For example, a rotation of  $\alpha$  corresponds to a phase angle  $3\alpha$  for a trefoil. Rotating the Zernike coefficients of the surface directly could introduce less fitting error than rotating the surface image rebuilt by the Zernike coefficients.

#### Optimum search detection

The simulation of wavefront rotation detection is performed using the experimental data from Section 4.1. The calculated modes #1 and #5 surfaces and their rebuilt surfaces are used. The rebuilt mode surfaces are rotated by a certain angle  $\theta$  to simulate the rotated wavefront surfaces of the rebuilt mode. Mode #1 is used for the main detection and mode #5 for the additional detection.

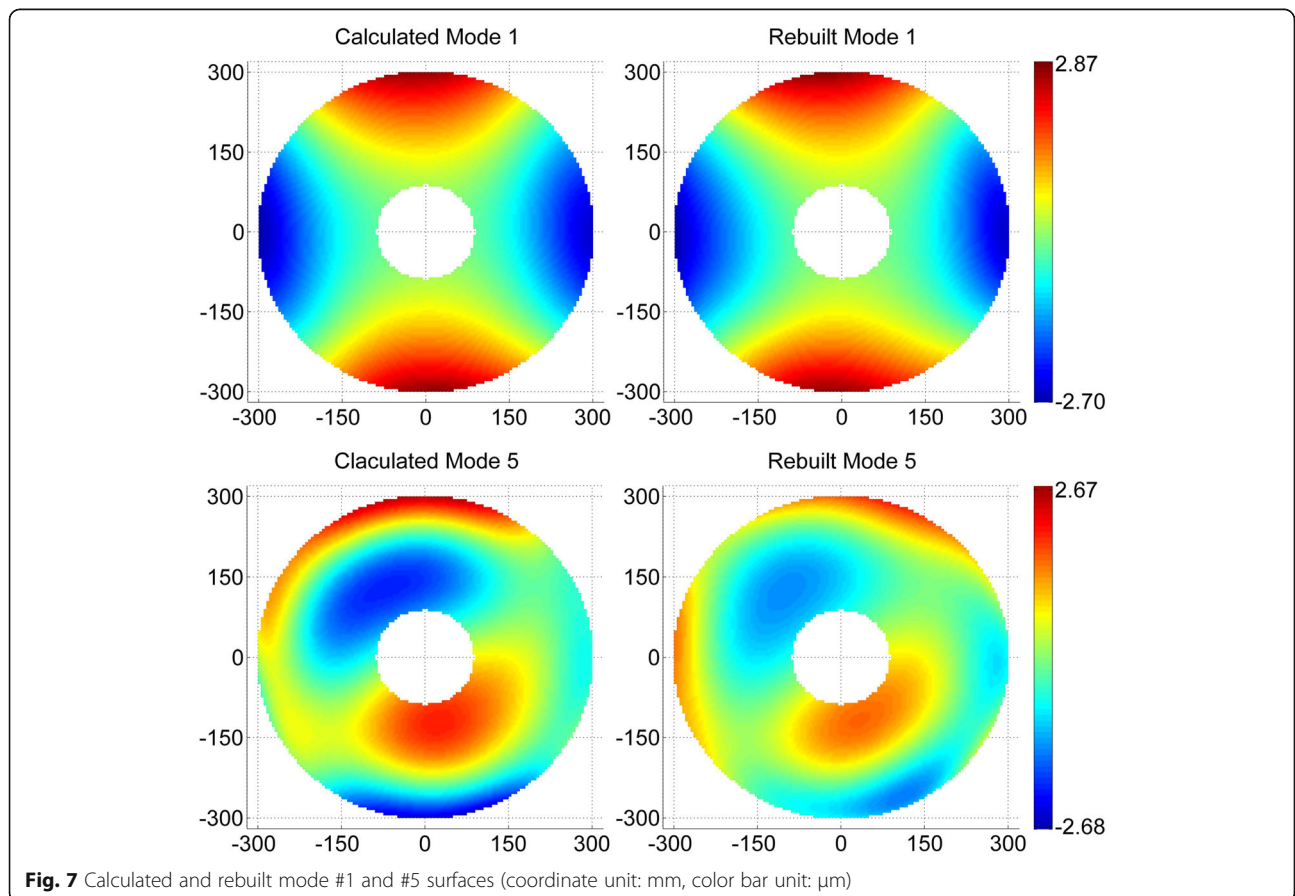
To detect the rotation angle of the two surfaces, an optimum search could be a suitable approach. The rotated wavefront surface is the search target. The calculated mode surface is rotated to fit the target, and the rotation angle  $\alpha$  is the parameter to be optimized. This is a simple two-way search. The optimum search begins with an initial rotation angle  $\alpha_0$ , an initial searching rate  $\phi_0$  and a rate scale factor

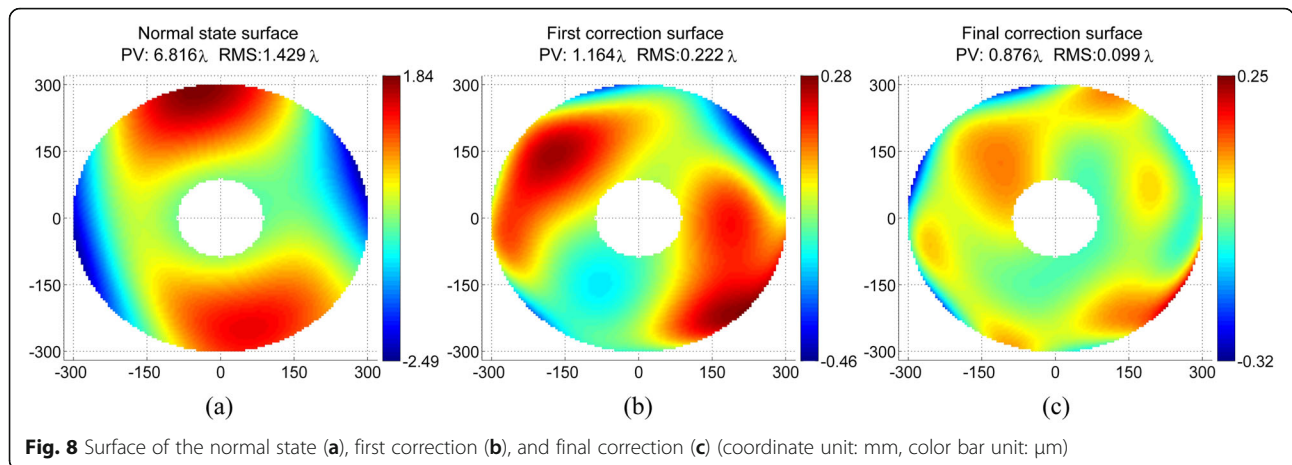




$\rho$ . In the searching step  $i$ , the calculated mode surface rotated by  $\alpha_i$  is compared with those rotated by  $\alpha_i + \phi_i$  and  $\alpha_i - \phi_i$ . If the mode surface rotated by  $\alpha_i + \phi_i$  or  $\alpha_i - \phi_i$  fits the target better, then  $a_{i+1} = a_i + \phi_i$  or  $a_{i+1} = a_i - \phi_i$ , and  $\phi_{i+1} = \phi_i$ . If it does not, then  $a_{i+1} = a_i$  and  $\phi_{i+1} = \rho \cdot \phi_i$ . The search is terminated after a certain number of searching steps or if the search rate  $\phi_i$  is less than a given value.

Comparison of each search step is performed using an evaluation function. The function evaluates the fitting of the rotated mode surface and target surface. The root mean square error (RMSE) and cross-correlation coefficient of the two surfaces and RMSE of the discrete cosine transform (DCT) of the two surfaces are tested as evaluation functions. The DCT image is transformed in  $4 \times 36$  blocks divided in polar coordinates.



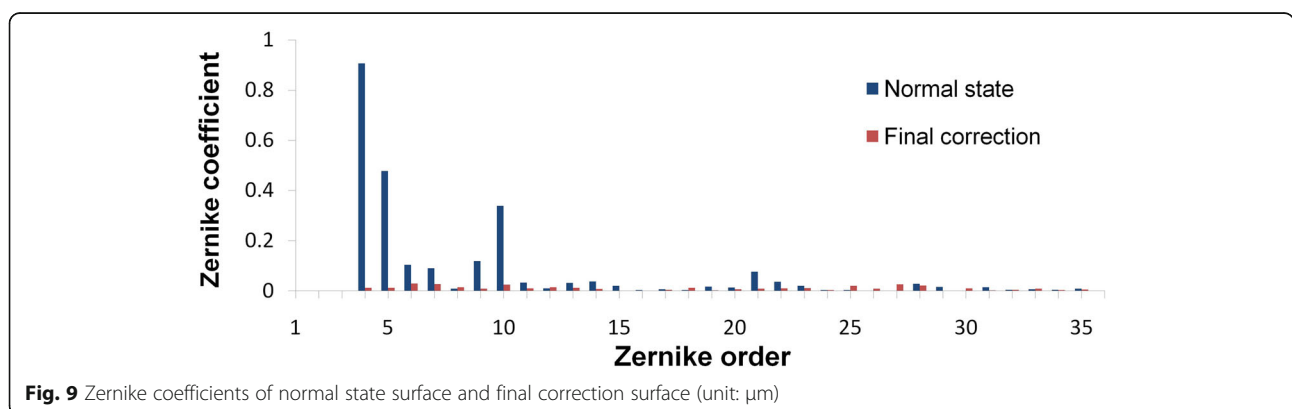


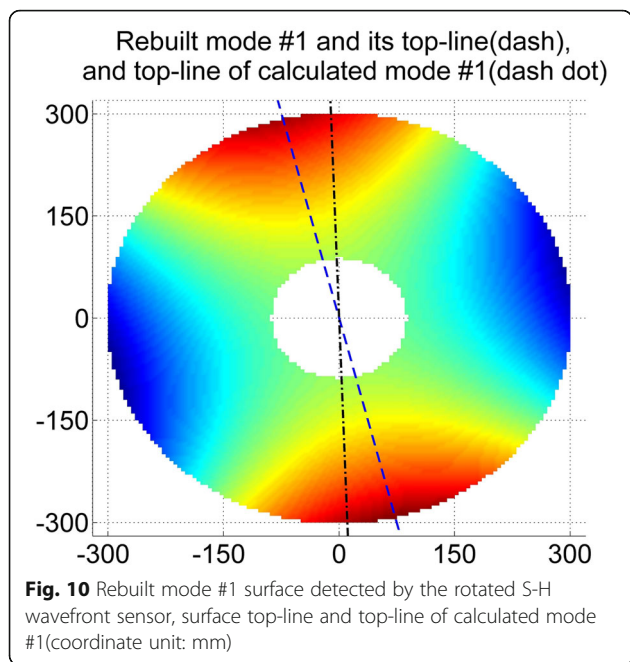
The simulation is set with  $\theta = 30^\circ$ ,  $\alpha_0 = 20^\circ$ ,  $\phi_0 = 22.5^\circ$ , and  $\rho = 0.8$ . The target surface is the rebuilt mode #1 surface rotated by  $\theta = 30^\circ$ . The first attempt is direct RMSE, which is to determine the RMSE of the rotated mode surface and target surface. The searching rate reduces to  $0.12413''$  in 100 steps, the searching result is  $\alpha = 29.714^\circ$ , and the detection error is  $0.286^\circ$ . Then, the DCT RMSE and cross-correlation coefficient are tested under the same conditions. However, the result of cross-correlation coefficient is  $\alpha = 29.691^\circ$ , which is close to that of direct RMSE, and the result of DCT RMSE is equal to that of direct RMSE. The detection error is mainly caused by the difference between the calculated mode surface and rebuilt mode surface. The searching value  $\alpha_i$  of the three evaluation functions is shown in Fig. 4, and they are almost the same. Direct RMSE, which requires less computation, is chosen as the evaluation function for the optimum search.

### Top-line detection

The precision of the optimum search is limited by the difference between the calculated mode and rebuilt mode. To obtain better detection for further correction, we use another approach based on the mode surface features. Mode #1 has two obvious aligned peaks. Then, a top-line that passes through the surface center and the tops of two peaks is selected for detection.

To identify the top-line, a series of rings, which are concentric with the surface, are set on the surface. The top-point of the two peaks on each ring is selected. The top-line angle is detected by a least mean square (LMS) fitting of these top-points. The angle between the top-lines of the source surface (calculated mode #1) and target surface (rotated rebuilt mode #1) is the detected rotation angle. The detection mainly depends on the features of the mode #1 surface, which are obvious and introduce





little detection error. This mode #1 top-line detection also involves the issue of 180° symmetry solution, and requires an additional detection to acquire the correct result.

The top-line detection is tested with the same simulation data used in Section 3.2. The target surface is still the rebuilt mode #1 surface rotated by  $\theta_0 = 30^\circ$ . The detection uses 44 rings to find 88 top-points. In each ring, the maximum point is found as the top-point of one peak, and a search in the opposite direction of this top-point is processed to detect the top-point of the other peak. Then, a top-line is detected by an LMS of these 88 top-points. The searching precision of the top-point is

1.40625''. The top-line angle of the calculated mode #1 surface is 92.028°, and that of the rotated rebuilt mode #1 surface is 121.943°. The detected rotation angle is 29.915°, and the detection error is 0.085°, which is much better than the values obtained in the optimum search. The calculated mode #1 and the rotated rebuilt mode #1 with their top-lines are shown in Fig. 5.

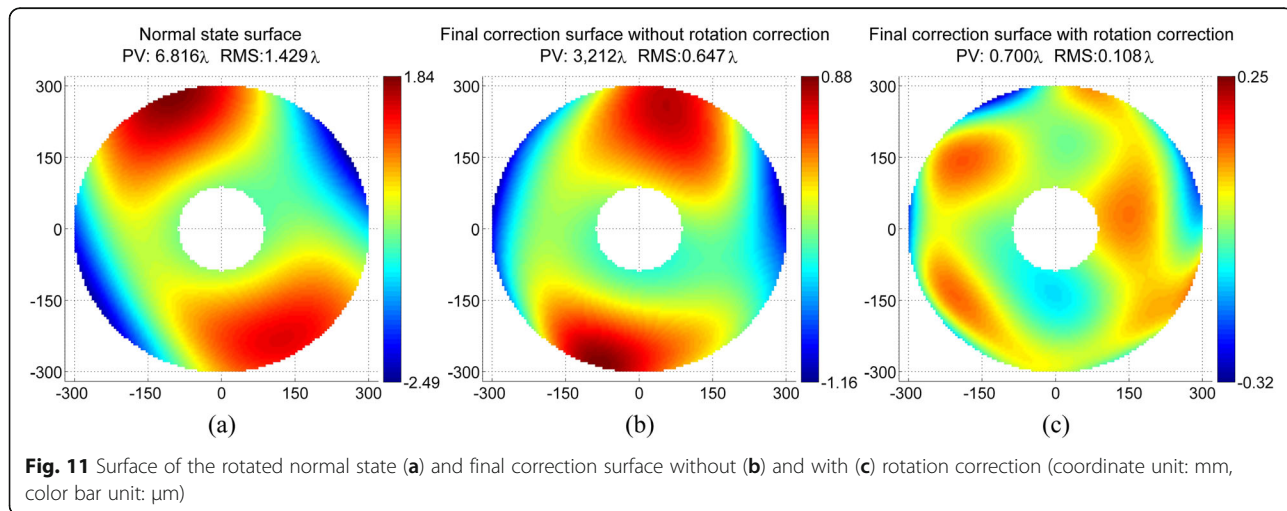
### Results of the experiments on 620-mm active optics system

#### Influence detection and mode rebuilding

The influence force used in the influence matrix measurement is a +10 N and -10 N balanced force. The influence function is obtained by the subtraction of two opposite surface deformations formed by adding +10 N and -10 N influence forces on actuators. Figure 6 shows the influence of the #1, #12 and #31 actuators, which correspond to the three actuator rings.

The bending mode and mode force of this active support system are calculated using the detected influence functions. A series of mode forces  $F_B$  is set on the active support to acquire the rebuilt mode surface. As a result, the first 6 modes can be well rebuilt on the system, and the rebuilt mode #1 is 92.1% similar to the calculated mode #1 in RMS. High order modes could be rebuilt as well, but they contain some low-order modes. Therefore, to obtain a good correction result, several correction iterations from high-order modes to low-order modes are performed.

The surfaces of calculated and rebuilt modes #1 and #5 are shown in Fig. 7, which are used in the rotation detection simulation. Calculated mode #1 and rebuilt mode #1 are very similar to each other and could result in good rotation detection, and mode #5 is the first asymmetric mode.



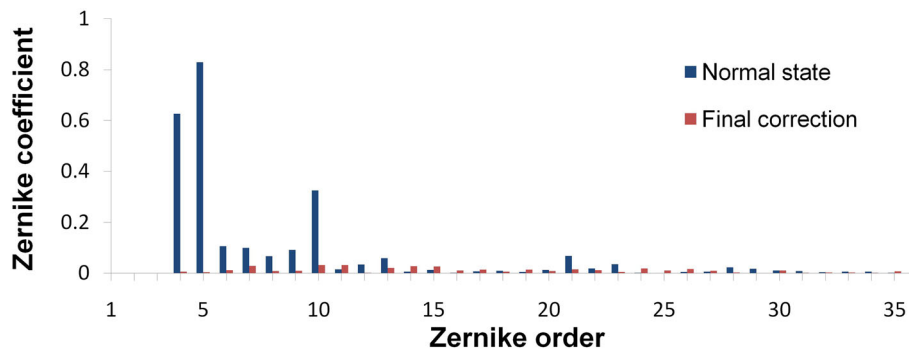


**Fig. 12** Zernike coefficients of normal state surface and final correction surface with rotation correction (unit:  $\mu\text{m}$ )

### Active correction using bending mode

The normal state surface of the mirror is shown in Fig. 8(a), where all the actuators are set to 0 N and the mirror is in a passive supported state. The surface has a large astigmatism. The first correction uses the first 15 modes to fit the surface and calculate the active force. The result is shown in Fig. 8(b), where the peak-to-valley (P-V) value and RMS of the surface are effectively reduced, but the astigmatism is still the main Zernike aberration. Then, two corrections using 12 modes and 2 modes are processed on the system and the result is shown in Fig. 8(c). As shown in Fig. 9, all the Zernike aberrations have been obviously corrected and the RMS is reduced to  $0.099\lambda$ . ( $\lambda = 632.5$  nm).

### Wavefront rotation detection

To obtain a rotated detection system, the camera of the S-H wavefront sensor is rotated by approximately  $10^\circ$ . Then, the detected wavefront surface is also rotated by approximately  $10^\circ$ . To achieve a good surface correction, the wavefront surface should be rotated back before fitting with bending modes.

First, the mode forces of modes #1 and #5 are added on the actuators to acquire the wavefront of the rebuilt mode. The rotation angle is detected using the top-lines of calculated mode #1 and the wavefront of rebuilt mode #1, as shown in Fig. 10. The detected result is  $11.950^\circ$ , which means that the rotation angle is  $11.950^\circ$  or  $191.950^\circ$ . Then the wavefront of rebuilt mode #5 is used to perform the additional detection by optimum search. The result is  $7.2908^\circ$ , which ensures that the detected rotation angle is  $11.950^\circ$ .

After rotation detection, the active correction in this rotated system has been performed. The normal state surface with all actuators set to 0N is detected, which has a large astigmatism and an obvious

rotation. First, a direct surface correction without rotation correction is performed on the rotated system. The result is not good; the mirror surface is  $0.647\lambda$  in RMS and still has a large astigmatism. Then, another correction process is started where the detected surface is rotated by  $-11.950^\circ$  before fitting with bending modes. The first correction is done in three iterations using 15 modes, 12 modes, and 2 modes. The correction result is  $0.108\lambda$  in RMS, similar to the result of the non-rotated detection system. The surfaces of the normal state and the two correction surfaces are shown in Fig. 11, and the Zernike coefficients of the normal state surface and final correction surface with rotation correction is shown in Fig. 12.

### Conclusions

A procedure for active correction and rotation detection using bending modes is described in this paper. Bending modes are a series of orthonormal modes arranged in increasing order of stiffness. These modes can be well rebuilt on an active optics system. Considering these characteristics, two rotation detection methods using bending modes were developed. These detection methods require no additional components and their detection precision is high. These two methods, namely optimum search and top-line detection, were firstly tested via simulation using experimental data from a 620-mm active optics system. The detection errors were  $0.286^\circ$  and  $0.085^\circ$ , respectively. Then, the rotation detection was tested on the 620-mm active optics system. Two active corrections were performed in non-rotation state and rotation state with top-line rotation detection. The similarity in such correction results means that the rotation detection is effective. In our future work, we plan to apply these rotation detection methods to the active optics system of a 4-m SiC primary mirror.

### Appendix

The influence matrix  $A$  is usually described in terms of Zernike coefficients. However, the wavefront of the primary mirror has a central hole, which means that Zernike polynomials are not orthogonal on the wavefront surface. Then, the issue is that mode  $B$  is orthonormal in Zernike coefficients but would not be on the wavefront of the primary mirror.

To address this problem, the influence matrix must be transferred to an orthonormal base before calculating the bending mode. Then, the SVD of the influence matrix is performed in the new orthonormal base to acquire the orthonormal bending mode  $B_V$  and its mode force. This operation preserves the orthonormal feature of the bending mode. There are many choices for the orthonormal base, as long as it has the same or more dimensions than the original Zernike polynomials base. Our choice is to perform a Gram-Schmidt orthogonalization on the Zernike polynomials  $Z$  to derive orthonormal polynomials  $V$ :

$$\begin{aligned} U_1 &= Z_1 \\ U_2 &= Z_2 + D_{21}U_1 \\ U_3 &= Z_3 + D_{31}U_1 + D_{32}U_2 \quad j = 2, 3, 4, \dots, n, \\ &\vdots \\ U_j &= Z_j + D_{j1}U_1 + D_{j2}U_2 + \dots + D_{j,j-1}U_{j-1} \end{aligned} \tag{8}$$

where

$$D_{ji} = -\frac{\int_{\epsilon}^1 \int_0^{2\pi} Z_j Z_i \cdot d\rho \cdot \rho \cdot d\theta}{\int_{\epsilon}^1 \int_0^{2\pi} Z_i^2 \cdot d\rho \cdot \rho \cdot d\theta}, j = 2, 3, 4, \dots, n, i = 1, 2, \dots, j-1 \tag{9}$$

$U$  is the orthogonal polynomials obtained from  $Z$ ,  $n$  is the max Zernike order, and  $\epsilon$  is the normalized radius of the central hole. Then,  $V$  is the normalized form of  $U$ ; that is,

$$V_i = U_i/U_{0i}, \quad U_{0i} = \int_{\epsilon}^1 \int_0^{2\pi} U_i^2 \cdot d\rho \cdot \rho \cdot d\theta. \tag{10}$$

Equation 10 can be expressed in terms of  $V$  and  $Z$  as

$$\begin{aligned} V_1 &= Z_1/U_{01} \\ V_2 &= Z_2/U_{02} + C_{21}Z_1 \\ V_3 &= Z_3/U_{03} + C_{31}Z_1 + C_{32}Z_2 \quad j = 2, 3, 4, \dots, n \\ &\vdots \\ V_j &= Z_j/U_{0j} + C_{j1}Z_1 + C_{j2}Z_2 + \dots + C_{j,j-1}Z_{j-1} \\ C_{ji} &= \frac{\sum_{s=1}^{j-1} D_{j,j-s} C_{j-s,i}}{U_{0j}} \quad i = 1, 2, \dots, j-1. \end{aligned} \tag{11}$$

Thus, the relationship between the Zernike coefficients  $z$  and the  $V$  coefficients  $v$  is

$$z = T*v, \quad v = T^{-1}*z$$

$$T = \begin{bmatrix} 1/U_{01} & C_{21} & & \dots & C_{n1} \\ 0 & 1/U_{02} & C_{32} & \dots & C_{n2} \\ \vdots & 0 & \ddots & \ddots & \vdots \\ 0 & \dots & & 1/U_{0\ n-1} & C_{n\ n-1} \\ & & & 0 & 1/U_{0\ n} \end{bmatrix}. \tag{12}$$

where  $T$  is the  $n \times n$  transformation matrix, which could be calculated using Zernike polynomials  $Z$  and the normalized central hole radius  $\epsilon$ .

If the new bending mode  $B_V$  is converted back to the Zernike base mode  $B$ , the Zernike coefficient vectors of  $B$  would be non-orthogonal. This means that fitting a surface aberration of a Zernike coefficient is not  $b = B^T * W$  but rather  $b = (B^T B)^{-1} B^T * W$ , and the fitting residual is minimized in the Zernike coefficient but not minimized in the primary surface deformation. A better method is to convert  $W$  to the orthonormal base by  $W_V = T^{-1} * W$  and use the orthonormal base mode  $B_V$  to fit  $W_V$ . Then, the fitting becomes  $b = B_V^T * W_V$  and the fitting residual is minimized in the orthonormal base, thus relating to the primary surface deformation.

#### Abbreviations

DCT: discrete cosine transform; LMS: least mean square; RMSE: root mean square error; S-H: Shack-Hartmann; SORT: Starfire Optical Range Telescope; SVD: singular value decomposition

#### Acknowledgements

Not applicable.

#### Authors' contributions

YZ, TC and HL conceived the presented idea. YZ developed the methodology. YZ and HL collected and analyzed the data. YZ discussed the result and wrote the paper. TC supervised the entire work. All authors read and approved the final manuscript.

#### Funding

Not applicable.

#### Availability of data and materials

Not applicable.

#### Competing interests

The authors declare that they have no competing interests.

Received: 21 August 2019 Accepted: 13 December 2019

Published online: 16 January 2020

#### References

- Martin, H.M., et al.: Active supports and force optimization for a 3.5-m honeycomb sandwich mirror. *SPIE*. **2199**, 251–262 (1994)
- Martin, H.M., et al.: Active supports and force optimization for the MMT primary mirror. *Proc. SPIE*. **3352**, 412–423 (1998)
- Schechter, P.L., et al.: Active Optics on the Baade 6.5-m (Magellan I) Telescope. *Proc. SPIE*. **4387**, 619–627 (2003)
- Martin, H.M., Cuerden, B., Dettmann, L.R., Hill, J.M.: Active optics and force optimization for the first 8.4 m LBT mirror. *Proc. SPIE*. **5489**, 826–837 (2004)
- Smith, B., et al.: The active optics system for the Discovery Channel telescope. *Proc. SPIE*. **7739**, 77391T (2010)
- Wang, Y., Silva, D.E.: Wave-front interpretation with Zernike polynomials. *Appl. Opt.* **19**, 1510–1518 (1980)

7. Abdelsalam, D.G., Baek, B.J., Kim, D.: Curvature measurement using phase shifting in-line interferometry, single shot off-axis geometry and Zernike's polynomial fitting. *Optik*. **123**, 422–427 (2012)
8. Smith, B., Cuerden, B.: Bending modes for active optics. *Proc. SPIE*. **8149**, 81490D (2011)
9. Noethe, L.: Active optics in modern, Large Optical Telescopes. *Progress in Optics*. **43**, 1–69 (2002)

### Publisher's Note

Springer Nature remains neutral with regard to jurisdictional claims in published maps and institutional affiliations.

**Submit your manuscript to a SpringerOpen<sup>®</sup> journal and benefit from:**

- ▶ Convenient online submission
- ▶ Rigorous peer review
- ▶ Open access: articles freely available online
- ▶ High visibility within the field
- ▶ Retaining the copyright to your article

---

Submit your next manuscript at ▶ [springeropen.com](https://www.springeropen.com)

---